Ultramicroscopy 155 (2015) 55–61

Contents lists available at ScienceDirect

Ultramicroscopy

journal homepage: www.elsevier.com/locate/ultramic

Methods for topography artifacts compensation in scanning thermal microscopy

Jan Martinek [a,c,*], Petr Klapetek [a,b], Anna Charvátová Campbell [a]

[a] Czech Metrology Institute, Okružní 31, 638 00 Brno, Czech Republic
[b] CEITEC, BUT, Technická 3058/10, 616 00 Brno, Czech Republic
[c] Department of Physics, Faculty of Civil Engineering, BUT, Žižkova 17, Brno 602 00, Czech Republic

ARTICLE INFO

Article history:
Received 10 July 2014
Received in revised form
8 April 2015
Accepted 15 April 2015
Available online 25 April 2015

Keywords:
Scanning thermal microscopy
Artifacts
Neural networks

ABSTRACT

Thermal conductivity contrast images in scanning thermal microscopy (SThM) are often distorted by artifacts related to local sample topography. This is pronounced on samples with sharp topographic features, on rough samples and while using larger probes, for example, Wollaston wire-based probes. The topography artifacts can be so high that they can even obscure local thermal conductivity variations influencing the measured signal. Three methods for numerically estimating and compensating for topographic artifacts are compared in this paper: a simple approach based on local sample geometry at the probe apex vicinity, a neural network analysis and 3D finite element modeling of the probe–sample interaction. A local topography and an estimated probe shape are used as source data for the calculation in all these techniques; the result is a map of false conductivity contrast signals generated only by sample topography. This map can be then used to remove the topography artifacts from measured data or to estimate the uncertainty of conductivity measurements using SThM. The accuracy of the results and the computational demands of the presented methods are discussed.

1. Introduction

Scanning thermal microscopy (SThM) is a member of the family of scanning probe microscope (SPM) techniques allowing us to measure temperature and heat transfer phenomena at the micro- and nanoscale [1,2]. The technique is based on the use of a local heater and/or temperature sensor, either in the form of a microfabricated probe or a very thin wire bent to form a probe. Scanning with this probe is performed using a conventional SPM feedback mechanism; the microscope can therefore measure sample topography and thermal properties at the same time.

From a theoretical point of view, SThM is not yet fully described as there are many physical phenomena taking place at the same moment during the experiment. The characteristic dimensions of objects playing a role here are comparable or even smaller than the mean free path of phonons, the contact thermal resistance of the generally rough probe and samples is unknown, the surface contamination effects are difficult to estimate and the influence of air and the adsorbed water layer is not easily predictable. Thus calibrating SThM either for temperature or for thermal conductivity measurements and interpreting the results are therefore not easy tasks. All these effects are the subject of intensive studies by many scientific groups all over the world [4–8]. The aim of this paper is not to supplant this effort, but to discuss some physically simple and practically usable approaches for making the interpretation of SThM data easier in daily tasks.

Topography artifacts in SThM are related to the variance of the probe's contact area depending on the local sample geometry and on the variance of the sample volume where heat can flow into different parts of the sample. If the probe is located, for example, on the edge of a flat sample surface, we can expect that the heat flow between the probe and the sample will be approximately twice lower compared to the heat flow when the probe is at the center of the sample since the probe–sample contact area on the edge is twice as small and there is less material in the probe vicinity to where heat could flow. On real samples the probe–sample area varies rapidly due both to microscale objects that may be on the surface and random roughness that is present nearly everywhere. This can lead to the rather complex behavior of the thermal conductivity contrast signal, namely when measured with larger probes. Typical topography artifacts are shown in Fig. 1. In Fig. 1A and B an image of the topography and conductivity contrast signal on a microchip surface covered with an aluminum layer is shown; i.e. the ideal thermal conductivity signal should be constant all over the sample. In Fig. 1C and D, the same set of signals for a solar cell surface close to a metallic contact is shown. Here an ideal

* Corresponding author at: Czech Metrology Institute, Okružní 31, 638 00 Brno, Czech Republic.

http://dx.doi.org/10.1016/j.ultramic.2015.04.011
0304-3991/

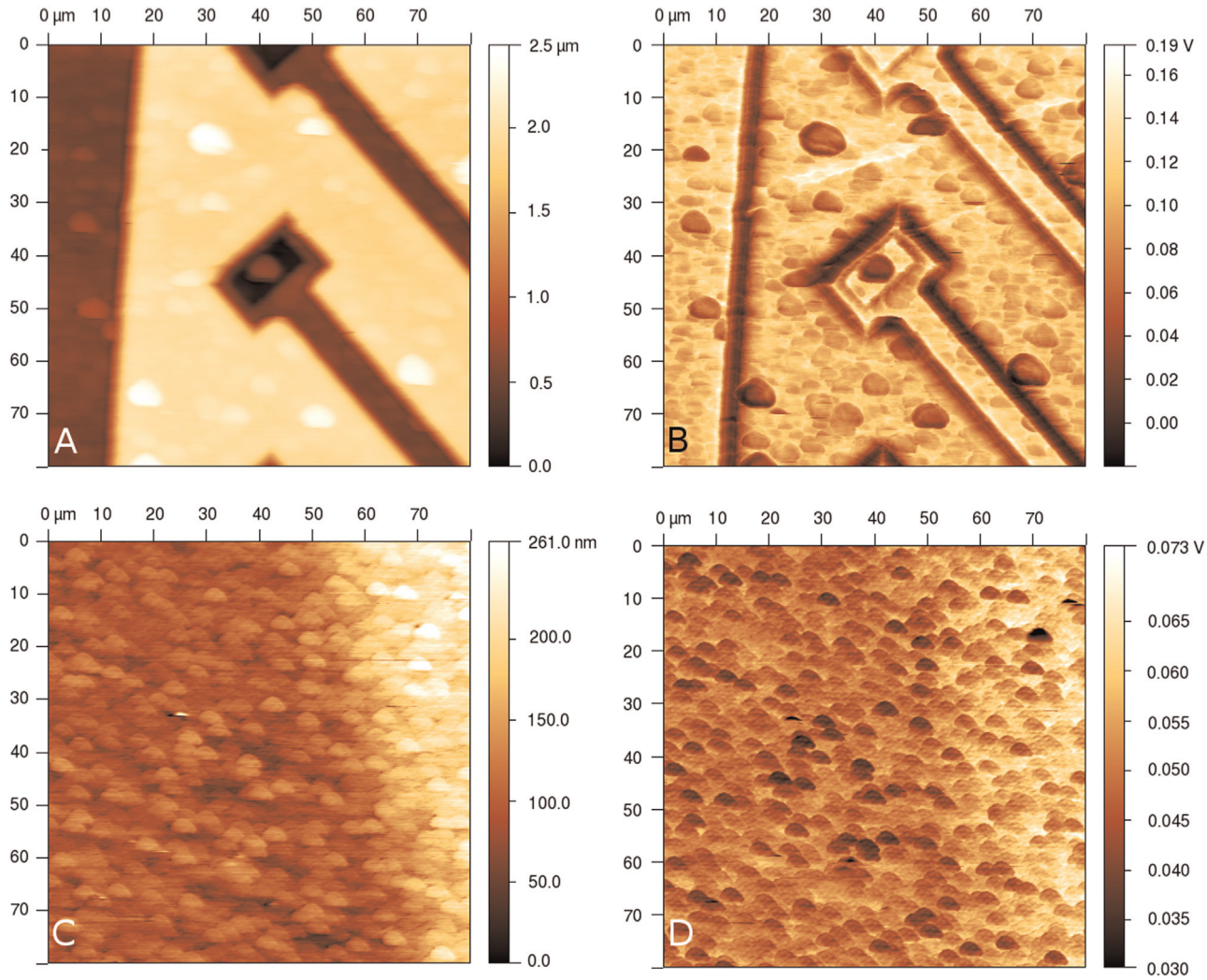

Fig. 1. SThM images showing characteristic artifacts: microchip surface covered by aluminum (A) topography and (B) conductance contrast signal, solar cell sample (C) topography and (D) conductance contrast signal.

thermal image would show two distinct areas, one without contact and one with contact. We can see that in both cases (Fig. 1B and D) the influence of the topography on the thermal conductivity signal is rather pronounced.

The aim of this paper is to compare different techniques for the estimation and removal of topography related artifacts in conductivity contrast scanning thermal microscopy data. We follow up on our previous work [9] and Ref. [11] where a neural network was used for topography artifact estimation, extending it by a larger variance of methods and comparing the results to finite element analysis under the assumption that diffusive regime conductivity treatment is enough to get an estimate of topography related artifacts.

2. Experimental arrangement

For all the SThM measurements an atomic force microscope explorer (Thermomicroscopes) with an SThM extension was used. Standard Wollaston wire (5 µm diameter) thermal probes were employed for thermal measurements. The conductivity contrast mode was used for all the measurements within this work. This mode is based on the use of a Wheatstone bridge acting as a probe resistance sensor and a feedback loop regulating the voltage applied on the bridge to keep the probe resistance constant. The probe resistance depends on its temperature, thus the feedback loop also acts as a thermostat keeping the probe temperature constant. The signal to be measured is the voltage applied to the

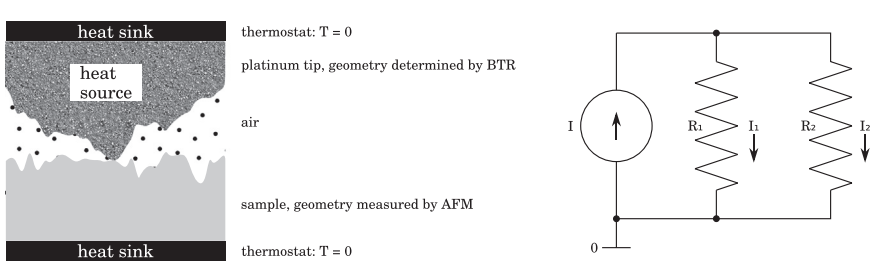

Fig. 2. The heat generated inside the tip flows into the ambient environment though the sample, but also by means of other mechanisms. On the right there is electrical schematics based on analogy between heat and electricity.

bridge. The voltage depends on the local heat flow from the probe to the sample. The controlling circuitry of the microscope deals with the overall electrical resistance of the probe. This signal is sufficient for the feedback to be functional, regardless of the fact that the temperature (and resistance) varies spatially within the probe.

Practically, the data measured using SThM are commonly used to calculate the thermal conductivity of a material being tested. For this reason, in the context of SThM the term thermal conductivity (or thermal conductivity contrast) is used in reference to SThM even though, strictly speaking, the measured value is thermal conductance, not conductivity.

To investigate the effects of the topography on the thermal conductivity signal we have first used a sample with homogeneous material properties. For this we have used a microchip covered by an aluminum layer providing both material homogeneity (assuming that the aluminum layer conducts much more than the structures specified below) and a complex topography.

Second, we have studied metallic contacts on the backside of a p–i–n solar cell. Solar cells were deposited by RF glow discharge in the ARCAM reactor [12]. The backside of the electrode, which consists of a Cr layer deposited on silicon, was studied. The edge of the electrode can be seen on the right side of image C in Fig. 1.

For FEM calculations, we used a high performance computing system from IBM with a ScaleMP virtual symmetric multiprocessor environment. The system has 10.5 TFlops of computational power and 6 TB of RAM. For other numerical methods a standard desktop computer was used.

All the calculations rely on input data representing the thermal conductivities of materials present in the sample. The following table lists the values used in the computations:

Material	**Thermal conductivity** λ (W/m/K)
Platinum (Pt)	71.6
Aluminum (Al)	237
Chromium (Cr)	93.9
Silicon (Si)	149
Air	0.026

3. Data processing

We have used three different techniques for the estimation of a thermal conductivity-related signal from local or global sample topography. The basic schematics showing their differences are shown in Fig. 3, the techniques are described in more detail below.

3.1. Neighbor volume technique

As a very simple technique for estimating topography artifacts, we performed the local evaluation of a sample material volume in the neighborhood of the probe. We can expect that when more sample material is in vicinity of the probe apex, the heat flow from the probe to the sample is larger. This effect corresponds to what we would expect and what we actually see on conductivity contrast images of simple structures like steps or particles. The evaluation was performed using the following steps implemented in Gwyddion software for SPM data processing [13]:

(1) Using the blind tip estimation algorithm [14] the tip shape was determined from the topography data.
(2) Surface reconstruction was used to get the real surface shape.
(3) The measured surface was used to determine the tip contact point. Then the reconstructed surface, which is considered to be real, was used for evaluation. The volume in close vicinity to the contact point was summed with a weight of $1/r^2$ where r is the distance from where the tip touches the surface. This proportionality was used because it follows the inverse square law. In other words, the heat flux density is inversely proportional to the square of the distance from the source. The different amount of material included on different parts of the sample is schematically shown in Fig. 4.
(4) The resulting data are relative numbers so the final step was a linear transformation which adjusted the minimum and maximum value to be the same as in the measured data.

3.2. Neural network treatment

The use of a neural network is a general approach that can be used to generate any result from any source data, assuming that we have trained the network to do so. It can be therefore also be trained to estimate topography artifacts in conductivity contrast SThM on a homogeneous sample, if we have enough data to perform the training.

Here we have used a simple feedforward NN trained with a backpropagation algorithm as discussed in our previous work [9] and referring also to the first work by Price [11]. The network had an input layer consisting of height differences corresponding to the characterization of the closest neighborhood of certain points in the topography image, one hidden layer of typically 10–15 neurons and an output layer representing the modeled thermal output value (see Fig. 5). A neural network works best if trained on situations closely resembling the actual case of use. For this reason, the NN was trained on a different homogeneous part of the sample, measured by SThM, featuring the same material,

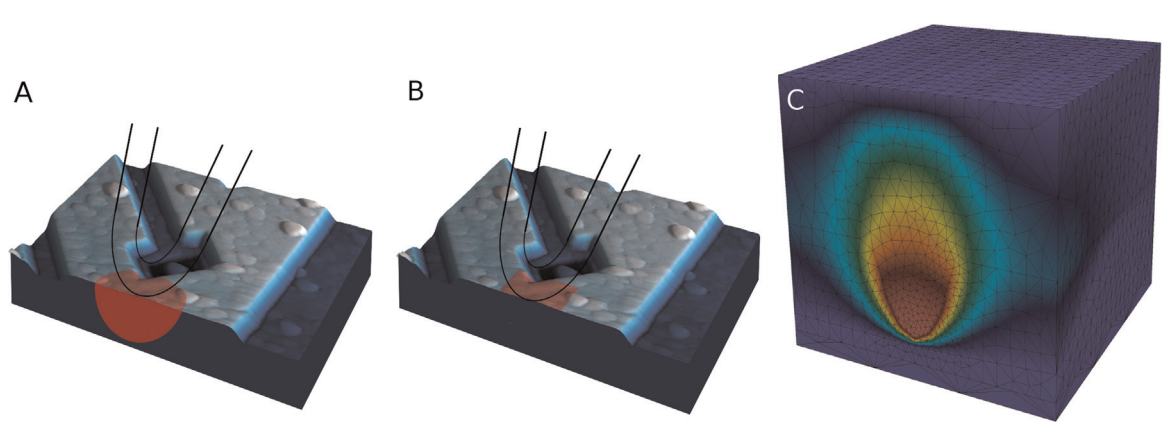

Fig. 3. Schematics of different artifact modeling techniques: (A) neighbor volume, (B) neural network, and (C) finite element analysis.

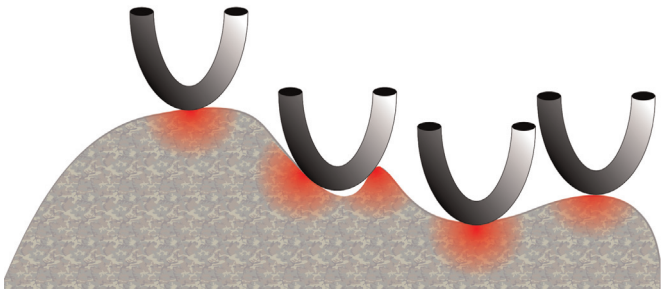

Fig. 4. Neighbor volume variations in different probe positions at the sample surface.

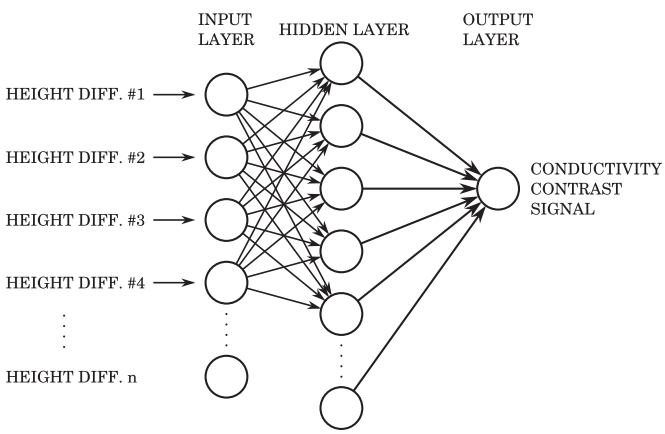

Fig. 5. Schema of the neural network used for thermal conductance signal estimation from height differences in sample topography close to the tip apex.

roughness and topography features. In this way it was able to estimate the apparent thermal conductivity signal value from the local neighborhood of the probe apex.

As the data are already trained on the measured conductivity contrast signal, the result values are also directly obtained in the range of the measured signal and are therefore directly comparable. Note that the same probe should be used for the acquisition of data for training and for the data that we are evaluating.

3.3. Finite element analysis

A finite element analysis was used to solve the Poisson equation related to diffusive heat transfer in the system, which is one of the popular approaches for SThM modeling in a diffusive regime [3,10].

One of the results of Fourier's law of thermal conduction is the main partial differential equation describing the heat flow. We assume a homogeneous material (or distinct homogeneous domains joined by boundary conditions) and therefore in any coordinate system the equation can be formulated as follows:

$$\frac{\partial T}{\partial t} - \alpha \nabla^2 T = 0$$

where the coefficient α represents the thermal diffusivity of a material, but due to the fact we assume a steady state of temperature field, this material property is canceled from the equation. Such an assumption leads to Poisson's equation:

$$\nabla^2 T = 0$$

Solving the equation results in a temperature field, which can be further used for the calculation of the heat flux:

$$\vec{q} = -\lambda \Delta T$$

The overall rate of heat flow passing through an area can be calculated by integrating the heat flux over the area:

$$P = \int_S \vec{q}\, \mathrm{d}\vec{S}$$

These equations represent the main tools for the finite element method. The geometry of the problem and the boundary conditions were chosen to resemble the reality but only major effects are taken into consideration due to the limitation of computing power. Also, many effects cannot be precisely quantified. The schematics of the model are depicted in Fig. 2 and the important features are as follows:

(1) Fixed temperature at the bottom of the sample, which represents the ambient conditions.
(2) The constant power density generated within the volume of the tip. This models the heat power P generated by the electric current.
(3) Fixed temperature at the upper part of the tip. The power generated within the tip flows partially into the sample (power P_1), but also partially to the environment (power P_2) via radiation, convection, conduction by the Wollaston wire etc. The purpose of this boundary condition is to model, at least, a phenomenological heat sink which dissipates part of the heat. Unfortunately, the exact amount cannot be determined with any certainty.
(4) The heat partially flows directly into the ambient environment and partially through the air into the sample. To avoid singularities, there was an air gap introduced between the very tip and the sample surface. Its value was set to be as small as possible to ensure numerical stability and its dimension is 1 nm.

The goal of the computation is to determine the thermal resistance R_1 between the tip and the bottom of the sample, but due to many unknowns only a value which is *in linear relationship* to the resistance is calculated.

The thermal resistance is a property measured in Kelvins per Watt which describes a rate of heat flow between two places with a given temperature difference. In our case it is not straightforward to use this idea because the temperature field within the heated tip is not uniform. Another approach was used to completely avoid the term “tip temperature”. It might be easier to show the principle on equivalent electrical schematics on the right of Fig. 2. The current I from the source splits into two branches, one passing through the resistor R_1 and the other passing through R_2. It can be shown that

$$R_1 = R_2\left(\frac{I}{I_1} - 1\right)$$

and this equation has the property that it does not contain the voltage (or potential), thus if we switch from the electricity back to the heat representation, we get

$$R_1 = R_2\left(\frac{P}{P_1} - 1\right)$$

which can be re-written to

$$R_1 = a\frac{1}{P_1} - b$$

where a and b are some unknown constants. The important conclusion is that it is possible to calculate $1/P_1$, which is in a linear relationship with R_1, without using the tip temperature. The P_1 can be calculated using FEM as a rate of heat which flows into the bottom of the sample.

For FEM modeling we decided to use an open source solution to

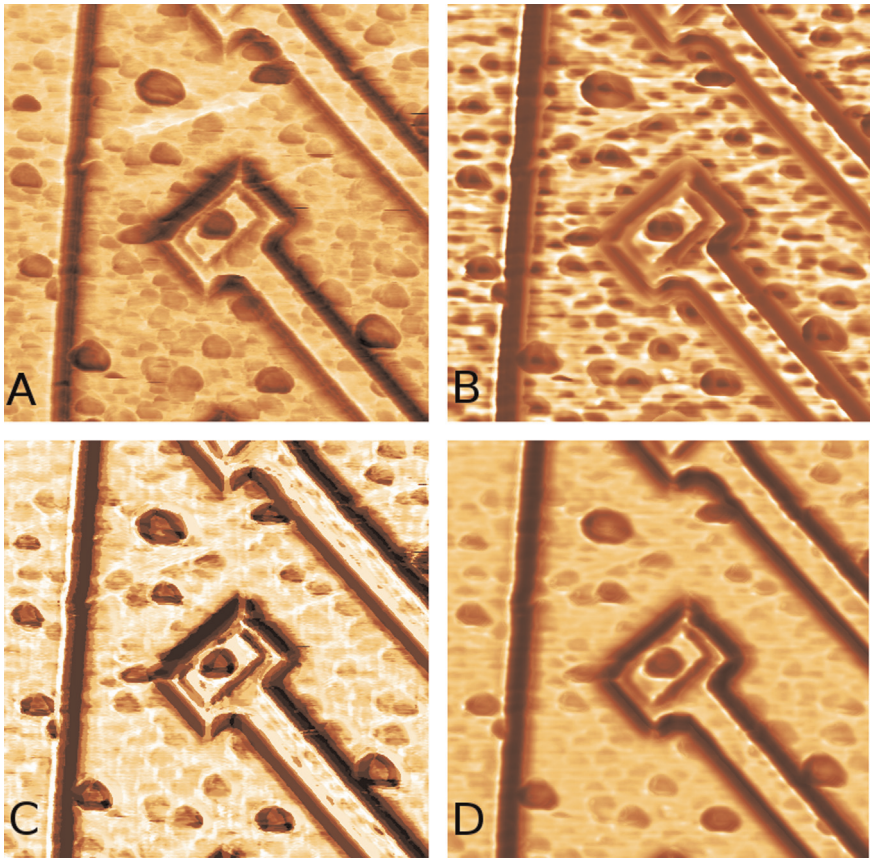

Fig. 6. Microchip surface conductance contrast signal: (A) measured, and evaluated from topography by (B) neighbor volume, (C) neural network and (D) finite element method.

have the possibility to modify the toolchain for our needs. Such an approach is not only free but also very flexible. We used a combination of the Python programing language [15] and Sfepy [16]. Sfepy is a Python module which supports finite element modeling. It is not standalone software; it is more or less a computation library for solving partial differential equations. It cannot calculate meshes but it does not matter as this task is previously done using GMSH software [17]. SfePy consumes the mesh data which come from GMSH, solves the equations and outputs the results into a *vtk file which can be displayed by any suitable viewer. Any data post-processing can be programed in Python which is quite a convenient way. In Python there is also a SciPy library intended for scientific purposes which makes the task even easier.

The finite element method (FEM) was used to calculate a steady state of temperature field on a geometry given by measured topography data and a tip shape calculated by blind tip reconstruction (BTR). The thermal conductivities of three materials were used in the model: platinum (the tip), the substrate and thin separating layer of air. The tip was modeled as a volumetric source of heat power (not isothermal). For each data point of the resulting thermal image the geometry and the mesh is different, because the tip position changes. The calculation was very demanding even for a supercomputer.

For the modeling using the finite element method there were several different types of software used. The tessellation of a given volume into a tetrahedral was done using GMSH software. The governing partial differential equations were solved by SfePy, which is a library intended for solving FEM problems in Python. Besides these two main types of software, several others made in-house were also programed. Each pixel in the final image was calculated by this scheme:

- Load the AFM topography data.
- Crop the topography to get a square of 21×21 pixels ($4.2\ \mu m \times 4.2\ \mu m$) while the pixel-in-question is in the middle. This step makes the problem much smaller – it would not be feasible to calculate the whole sample in a reasonable time. We assume that points too far from the tip do not influence the result very much. The larger the cropped area the longer the computation time. Therefore, there is a compromise between speed and accuracy.
- The tip topography, which had been calculated before using blind tip reconstruction (BTR), is now used to calculate the contact point between the tip and the sample.
- As the mutual position of the tip and surface is now known, the geometry is tessellated using GMSH to get a tetrahedral mesh.
- The Poisson equation is solved on the mesh at the assumption that heat is generated in the tip at a constant rate of heat flow per volume element (in W/m^3). This approach models the reality better than simply setting the tip temperature at a fixed value. In reality, the electric current flows through the Wollaston wire and generates heat in its volume.
- The result of the calculation is a temperature field. The next step is to calculate the gradient of the field representing heat flux.
- The heat flux is integrated over the bottom part of the sample, which represents the heat sink. The result of the entire calculation is one number – the rate of heat flow in watts.

All the steps listed above had been done for each data point in the topography image except the areas too close to the boundary. From preliminary tests we concluded that the heat flow is not significantly influenced by areas further than 10 pixels (2 μm) away from the tip. As the resolution of the topography image was

400 × 400 pixels (80 μm × 80 μm), the safe area unaffected by edges has a resolution of 380 × 380 pixels (76 μm × 76 μm). This leads to solving 144 400 three dimensional FEM problems including mesh generation.

4. Results and discussion

In Fig. 6 the results of the calculation of thermal conductivity signal artifacts on a homogeneous sample using the three aforementioned methods are shown. A profile taken over a single strip on the sample is compared for all the techniques in Fig. 7. We can see that all the methods were able to basically estimate most of the topography related artifacts, however their applicability differs considerably:

- Neighbor volume technique can be used for a very fast but only coarse estimation of the effects of topography in the probe–sample contact region on apparent thermal conductivity. To get realistic results we need to estimate the probe shape and reconstruct the true sample topography, which is not possible on many samples (we need to have enough sharp features on topography to get the probe information). Another possibility to measure tip shape is using a special sample designed for this purpose.
- The neural network approach seems to be very fast and efficient. We do not need to estimate the probe shape and if the network is already trained the process is very fast. However, it is not an easy task to find good data for training the network and we cannot transfer a trained network for use with another probe or too different a sample surface. As this approach has nothing to do with any physical phenomena it can fail completely if the training goes wrong.
- The FEM analysis is the most complex and is the only one of the used approaches that includes some of the physics of tip-sample contact thermal resistance and heat flow through both the probe and sample. It is therefore computationally demanding and still not usable for daily use. Once again we need to know the probe shape and we need to estimate it even beyond the shape that can be estimated from the blind tip estimation, for example. Therefore some geometrical model of the tip needs to be constructed. On the other hand, we can evaluate more information from a complete FEM simulation, we can add a realistic sample structure, etc.

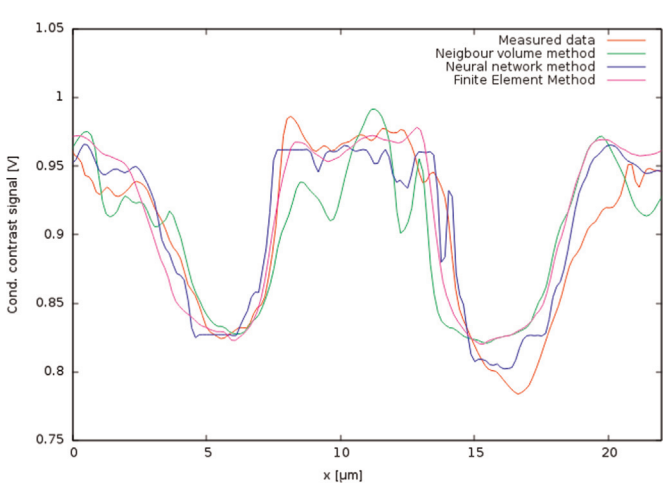

Fig. 7. Profile over step on microchip surface conductance contrast signal: (A) measured, and evaluated from topography by (B) neighbor volume, (C) neural network and (D) finite element method.

It should be noted again that the presented methods have significantly differing computational demands: from roughly 2 s that we need for applying a neural network (after some minutes of training it), through 10 s for a neighbor volume evaluation up to almost a day for a complete calculation using FEM.

We have also used all the methods to subtract their predicted topography artifacts from the real signal in order to correct the measured data. In Fig. 8 a result of this treatment is shown. Ideally, we would expect to see two adjacent areas of constant thermal conductivity contrast signal – the left part is the silicon, the right part is covered by a chromium layer. Possibly, there could be some gradient of the signal from left to right as the edge of the electrode is not steep enough. In Fig. 8A, as the whole sample is rough, there is a measured signal with many topography-related artefacts on it. The appearance is oval-shaped dark spots. The darker color corresponds to lower thermal conductivity.

The following table shows the standard deviation of values corresponding to a uniform part of the solar cell sample. Theoretically, the measured value (voltage) should be constant across the entire area thus the standard deviation (σ) should be equal to zero. In a real sample, suppressing the artifacts should lower the deviation.

Method	Time (s)	σ (mV)
Original data	*N.A.*	3.7
Neighbor volume	10	2.7
Neural network	2	2.6
FEM	80 000	1.5

We can see that after the subtraction of the simulated signal all the techniques can significantly improve the thermal image; the finite element method seems to be the most effective. On the other hand, it is by far the slowest method.

The scope of this paper is to test different methods to suppress topography artefacts on both homogeneous and heterogeneous samples. The next step might be to evaluate the numerical value of thermal conductivity, but a lot of effort would have to be made. One of the problems to consider is the evaluation of interfacial resistance between different materials, water meniscus effects, etc.

5. Conclusion

We have compared three methods for the calculation of a topography related signal in conductance contrast SThM imaging. Such calculations are useful for better understanding the image formation on complex sample geometries and for the estimation of the level of conductance signal distortion by the influence of sample topography.

The most complex method tested is to calculate the tip-sample heat flow in 3D for every pixel in the measured data based on the local topography (that is measured at the same time) and to compare the calculated results with conductance signal measurements. As this approach is very computationally demanding, a neural network can be used as an alternative that in special cases can provide nearly the same results as an FEM analysis while being much faster.

For practical use, a simple integration of the local sample volume in the vicinity of the probe apex can also be used, providing at least a first impression of where the topography artifacts will be observed and how they can influence the measured data. The results of this approach are far less accurate, though they can be obtained very quickly.

The estimated topography artifacts can be also used to make an estimation of uncertainties related to local probe–sample

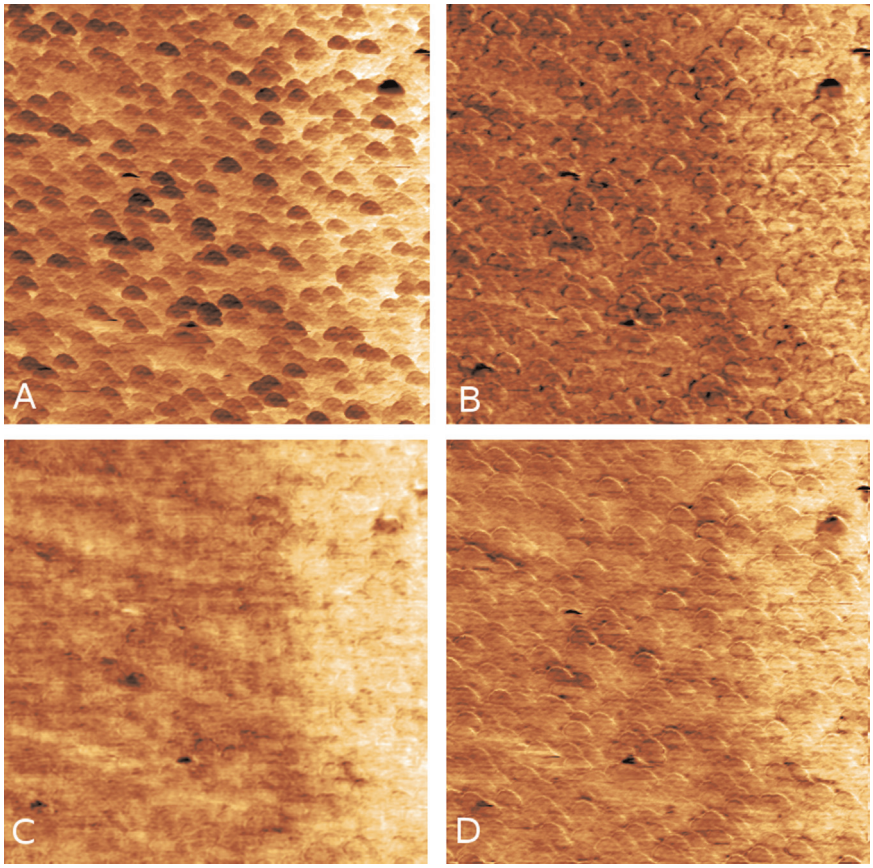

Fig. 8. Solar cell sample: (A) measured conductance contrast signal and corrected signal after artifact removal by (B) neighbor volume method, (C) neural network and (D) finite element method.

geometry changes while developing more quantitative SThM methods.

Acknowledgments

The research leading to these results has received funding from the European Union Seventh Framework Programme FP7-NMP-2013-LARGE-7 under Grant agreement no. 604668, and from Project FAST-S-15-2662.

References

[1] H.M. Pollock, A. Hammiche, J. Phys. D: Appl. Phys. 34 (2001) R23–R53.
[2] D.G. Cahill, K. Goodson, A. Majumdar, J. Heat Transf. 124 (2002) 223.
[3] A. Altes, R. Heiderhoff, L.J. Balk, J. Phys. D: Appl. Phys. 37 (2004) 952–963.
[4] H. Fischer, Thermochim. Acta 425 (2005) 69–74.
[5] S. Gómes, N. Trannoy, Ph. Grossel, F. Depasse, C. Bainier, D. Charraut, Int. J. Therm. Sci. 40 (2001) 949–958.
[6] S. Callard, G. Tallarida, A. Borghesi, L. Zanotti, J. Non-Cryst. Solids 245 (1999) 203–209.
[7] G. Wielgoszewski, P. Sulecki, P. Janus, P. Grabiec, E. Zschech, Th. Gotszalk, Meas. Sci. Technol. 22 (2011) 094023.
[8] F. Depasse, Ph. Grossel, N. Trannoy, Superlatt. Microstruct. 35 (2004) 269–282.
[9] P. Klapetek, I. Ohlídal, J. Buršík, Surf. Interface Anal. 38 (2006) 383–387.
[10] L. David, S. Gomés, M. Raynaud, J. Phys. D: Appl. Phys. 40 (2007) 4337–4346.
[11] D.M. Price, The Development and Applications of Micro-Thermal Analysis and Related Techniques (Ph.D. thesis), Loughborough University, Loughborough, 2002.
[12] P. Roca i Cabarrocas, J.B. Chévrier, J. Huc, A. Lloret, J.Y. Parey, J.P.M. Schmitt, J. Vac. Sci. Technol. A 9 (1991) 2331.
[13] D. Nečas, P. Klapetek, Cent. Eur. J. Phys. 10 (2012) 181–188.
[14] J. Villarubia, J. Res. Natl. Inst. Stand. Technol. 102 (2007) 425.
[15] ⟨http://python.org⟩.
[16] ⟨http://sfepy.org⟩.
[17] ⟨http://www.geuz.org/gmsh⟩.